ACSNANO
www.acsnano.org
ARTICLE

Highly Efficient Light-Emitting Diodes of Colloidal Metal–Halide Perovskite Nanocrystals beyond Quantum Size

Young-Hoon Kim,[†,‡,§] Christoph Wolf,[∥] Young-Tae Kim,[∥] Himchan Cho,[†,‡,§] Woosung Kwon,[⊥] Sungan Do,[#] Aditya Sadhanala,[△] Chan Gyung Park,[∥] Shi-Woo Rhee,[#] Sang Hyuk Im,[¶] Richard H. Friend,[△] and Tae-Woo Lee*[,†,‡,§]

[†]Department of Materials Science and Engineering, [‡]Research Institute of Advanced Materials, and [§]BK21 PLUS SNU Materials Division for Educating Creative Global Leaders, Seoul National University, 1 Gwanak-ro, Gwanak-gu, Seoul 08826, Republic of Korea

[∥]Department of Materials Science and Engineering, Pohang University of Science and Technology (POSTECH), Pohang, Gyungbuk 790-784, Republic of Korea

[⊥]Department of Chemical and Biological Engineering, Sookmyung Women's University, 100 Cheongpa-ro 47-gil, Yongsan-gu, Seoul 04310, Republic of Korea

[#]Department of Chemical Engineering, Pohang University of Science and Technology (POSTECH), 77 Cheongam-Ro, Nam-Gu, Pohang, Gyeongbuk 790-784, Republic of Korea

[△]Cavendish Laboratory, University of Cambridge, JJ Thomson Avenue, Cambridge CB3 0HE, U.K.

[¶]Department of Chemical and Biological Engineering, Korea University, 145 Anam-Ro, Seongbuk-Gu, Seoul 02841, Republic of Korea

Supporting Information

ABSTRACT: **Colloidal metal–halide perovskite quantum dots (QDs) with a dimension less than the exciton Bohr diameter D_B (quantum size regime) emerged as promising light emitters due to their spectrally narrow light, facile color tuning, and high photoluminescence quantum efficiency (PLQE). However, their size-sensitive emission wavelength and color purity and low electroluminescence efficiency are still challenging aspects. Here, we demonstrate highly efficient light-emitting diodes (LEDs) based on the colloidal perovskite nanocrystals (NCs) in a dimension > D_B (regime beyond quantum size) by using a multifunctional buffer hole injection layer (Buf-HIL). The perovskite NCs with a dimension greater than D_B show a size-irrespective high color purity and PLQE by managing the recombination of excitons occurring at surface traps and inside the NCs. The Buf-HIL composed of poly(3,4-ethylenedioxythiophene)/poly(styrenesulfonate) (PEDOT:PSS) and perfluorinated ionomer induces uniform perovskite particle films with complete film coverage and prevents exciton quenching at the PEDOT:PSS/perovskite particle film interface. With these strategies, we achieved a very high PLQE (~60.5%) in compact perovskite particle films without any complex post-treatments and multilayers and a high current efficiency of 15.5 cd/A in the LEDs of colloidal perovskite NCs, even in a simplified structure, which is the highest efficiency to date in green LEDs that use colloidal organic–inorganic metal–halide perovskite nanoparticles including perovskite QDs and NCs. These results can help to guide development of various light-emitting optoelectronic applications based on perovskite NCs.**

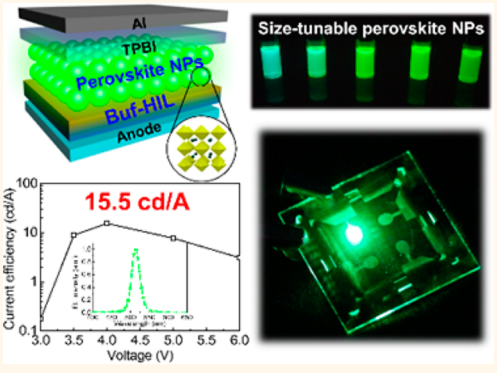

KEYWORDS: *perovskite nanocrystal, quantum size, light-emitting diodes, hole injection layer, electroluminescence*

Metal–halide perovskite emitters emerged as promising light emitters because they are inexpensive, can emit spectrally narrow light (full width at half-maximum (fwhm) ≈ 20 nm), which is irrespective of their grain/particle size, and have facile color tuning and comparable ionization energy (IE) and electron affinity levels with those of

Received: November 11, 2016
Accepted: June 6, 2017
Published: June 6, 2017

DOI: 10.1021/acsnano.6b07617
ACS Nano 2017, 11, 6586–6593

organic charge-transporting layers.[1−4] However, electroluminescence (EL) efficiencies based on conventional polycrystalline perovskite bulk films are limited by the low exciton binding energy (E_b) of the perovskite bulk films (*e.g.*, 76 meV for methylammonium lead bromide ($CH_3NH_3PbBr_3$)) and low photoluminescence quantum efficiency (PLQE) at room temperature (RT), by the presence of electrical shunt paths caused by the rough surface and pinholes in perovskite films and by the large number of intrinsic defects caused by imperfect micrometer-sized cubic crystals.[5,6]

Recently, the potential of polycrystalline perovskite bulk film emitters has been demonstrated by confining the exciton in small perovskite nanograins (~100 nm), reducing the exciton diffusion length, L_D (~67 nm), and leakage current in devices by fabricating a uniform perovskite film;[2,4] these results showed that the photoluminescence (PL) and EL efficiencies of perovskite emitters can be increased if E_b can be further increased and L_D can be decreased by reducing the grain size.

However, a more ideal approach to achieve high E_b and low L_D in perovskite emitters is to effectively confine the excitons in the form of nanometer-scale (<20 nm) colloidal perovskite nanoparticles (NPs) rather than in polycrystalline perovskite bulk films with large grain size (0.1−10 μm). These perovskite NPs are in totally different research subfields from polycrystalline perovskite bulk films and have completely different approach methods and fabrication processes.[7] Thus, development and application of perovskite NPs as emitters should be considered separately from those of polycrystalline perovskite bulk films. Furthermore, perovskite NPs can have a higher possibility to improve the EL efficiency of perovskite emitters than can polycrystalline perovskite bulk films because perovskite NPs themselves showed much higher PLQE than did polycrystalline perovskite bulk films.[2,6,7] Therefore, solution-processed light-emitting diodes (LEDs) based on perovskite NPs with size-irrespective high color purity and efficiency should be studied.

Perovskite NPs can be divided into two different regimes: (i) perovskite quantum dots (QDs) with a dimension less than the exciton Bohr diameter, D_B (quantum size regime), and (ii) unexplored perovskite nanocrystals (NCs) with a dimension greater than the D_B (regime beyond quantum size). Perovskite QDs with size less than D_B (<10 nm) showed high E_b and low L_D and thereby achieved high PLQE at RT.[6−12] In addition, the amenability of perovskite QDs to colloidal synthesis gives various advantages such as compatibility with shape- and size-engineering, compositional diversity, excellent solubility in common organic solvents (*e.g.*, toluene and chlorobenzene), and the possibility of postsynthetic reversible chemical exchange of halide anion.[6−12] However, these studies do not exploit the great advantage that electronic properties of perovskite emitters are determined by the unit crystal's structure rather than by the particle size and still suffer strong dependence of emission wavelength and color purity on the QD size, as do inorganic QDs.[13] Therefore, perovskite NCs with a dimension greater than the D_B in which the wavelength and color purity of the emitted light are not affected by the particle size should be evaluated.

Furthermore, uniform perovskite NC films should also be fabricated to demonstrate the high-efficiency LEDs. However, perovskite QD or nanoplate films on a conventional poly(3,4-ethylenedioxythiophene):poly(styrenesulfonate) (PEDOT:PSS) hole injection layer (HIL) induced the inhomogeneous surface morphology with pinholes and aggregated QDs or nanoplates and, thus, reduced the luminescence efficiency in LEDs.[14] Recently, uniform perovskite QD or nanoplate films and the potential of high-efficiency LEDs were demonstrated by covering the perovskite nanoplate films with organic host materials or by using trimethylaluminium vapor-based cross-linking methods or by using dip-coating methods to fabricate the QD films on a PEDOT:PSS/poly(9-vinylcarbazole) multilayer.[14−16] Very recently, efficient LEDs based on colloidal perovskite nanoplate films were also demonstrated (external quantum efficiency (EQE) = 0.23% for blue-sky, EQE = 0.038% for violet, and EQE = 2.31% for green),[17,18] and the highest current efficiency (CE) reported so far in green LEDs that use colloidal organic−inorganic metal-halide perovskite NP layers is 11.49 cd/A.[19] The exciton quenching by PEDOT:PSS at the PEDOT:PSS/perovskite NP interface in the devices can still be significant.[3] The device efficiency can be further improved by overcoming the severe exciton quenching at the PEDOT:PSS/perovskite NP interface and by fabricating the uniform perovskite NP films with complete film coverage.[20] Therefore, homogeneous perovskite NC films without any additional processes and multilayers need to be fabricated and the exciton quenching at the PEDOT:PSS/perovskite NC interface should be prevented to further improve the EL efficiency of perovskite NC-LEDs.[20]

Here, we report the highly efficient perovskite NC-LEDs by two important strategies: (i) synthesizing the $CH_3NH_3PbBr_3$ NP emitters with dimensions greater than the D_B (perovskite NCs) and (ii) using a multifunctional buffer hole injection layer (Buf-HIL) (Figure 1a,b). Perovskite NCs (*i.e.*, perovskite NPs with dimensions greater than the D_B) unlike QDs lead to size-insensitivity of the emission wavelength and of color purity, due to crystal-structure-dependent electronic band structures.[1,2] Furthermore, they can also achieve high PLQE and EL efficiency because NCs have a lower surface area to volume ratio and, therefore, show less trap-assisted recombination occurred at the surface traps and a smaller amount of insulating ligand in film states than do perovskite QDs (dimensions less than the D_B).[6,8,21,22] Buf-HIL also induces uniform perovskite particle films with complete film coverage. Furthermore, they can prevent exciton quenching at the PEDOT:PSS/perovskite particle film interface.[3] With these strategies, we achieved a very high PLQE (~60.5%) in compact perovskite particle films without any complex post-treatments and a high CE of 15.5 cd/A in perovskite NC-LEDs even in a simplified device structure (anode/Buf-HIL/perovskite NCs/1,3,5-tris(*N*-phenylbenzimiazole-2-yl)benzene (TPBI)/cathode).

RESULTS AND DISCUSSION

We used solubility-difference-assisted crystallization at RT to synthesize $CH_3NH_3PbBr_3$ NPs with various sizes including QDs and NCs that incorporate two ligands: (1) *n*-hexylamine to prevent the direct crystallization of $CH_3NH_3PbBr_3$ precursors into large (micrometer) crystals when they are mixed with "bad" solvent (*e.g.*, toluene) and (2) oleic acid to suppress the reaggregation of synthesized perovskite NPs and to control the crystallization rate and size of the particle by adhering to the surfaces of perovskite NPs.[6,8,23] This adhesion is facilitated by charge equilibrium between carboxyl groups of oleic acid and amine groups of methylammonium in perovskite NPs.[6] Oleic acid can serve as an emulsifier and surface-capping agent by anchoring to the surface amine groups of perovskite NPs. Thus, we can control the size of perovskite NPs by adjusting the amount of oleic acid: increasing the amount of

DOI: 10.1021/acsnano.6b07617
ACS Nano 2017, 11, 6586−6593

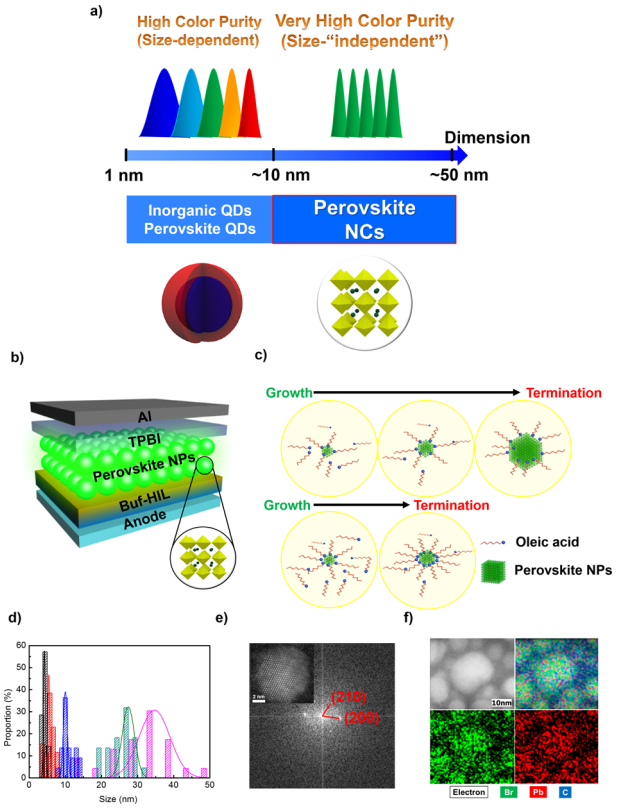

Figure 1. (a) Dimension distributions of inorganic QDs, perovskite QDs, and perovskite NCs, (b) device architecture of perovskite NP-LEDs, (c) schematic illustration of size-controllable perovskite NP synthesis, (d) size distribution histogram of perovskite NPs according to the different amount of ligand quantity, (e) fast Fourier transform pattern and high-resolution TEM image (inset), and (f) elemental mapping of perovskite NPs.

emulsifier oleic acid reduces the duration of the reaction and thus decreases the NP size from ~35 nm to ~3 nm and reduces the size deviations (Figure 1c,d and Figure S1).[23−25] High-resolution transmission electron microscopy (HR-TEM) and the fast Fourier transform (FFT) image showed a good crystalline structure with interplanar distances of 2.68 and 2.95 Å, which correspond to the (210) and (200) crystal planes, respectively (Figure 1e); this observation indicates that perovskite NPs had a cubic $Pm\bar{3}m$ phase. These crystal planes are consistent with the X-ray diffraction (XRD) peaks, which can be interpreted using Bragg's law (Figure S2). The broad XRD peaks according to the Debye−Scherrer expression further confirm that the perovskite NPs are small.[8] Elementary mapping images measured by energy dispersive spectroscopy (EDS) further confirm that Pb and Br atoms that constitute the perovskite crystals are uniformly distributed in their perovskite NPs (Figure 1f).

By fitting an equivalent circuit model of impedance spectroscopy data, we extracted the exciton Bohr radius, $r_B \approx 5$ nm, which is in accordance with previous literature (Figure S3).[26−28] This result indicates that perovskite NPs < 10 nm (*i.e.*, QDs) showed a blue-shifted PL spectrum (484 nm for 5 nm QDs and 470 nm for 3 nm QDs, respectively) due to the quantum-size effect and a broadened PL spectrum (fwhm: 35 nm for 5 nm QDs and 30 nm for 3 nm QDs, respectively) possibly due to the size distribution and to defect states or shallow traps in the large surface regions (Figure 2a,b).[22] These blue-shifted PL spectra of perovskite QDs indicated the increasing PL peak energy with decreasing dimension below the quantum size ($<D_B$); these are consistent with the effective mass theory for semiconductor QDs (Figure S4).[26,27,29] The PL spectrum of perovskite NPs > 10 nm (*i.e.*, NCs) showed sharp peaks (fwhm ~23 nm) at ~515 nm. These perovskite NCs are beyond the quantum-size regime, and their spectrum is unaffected by their particle size because their electronic band

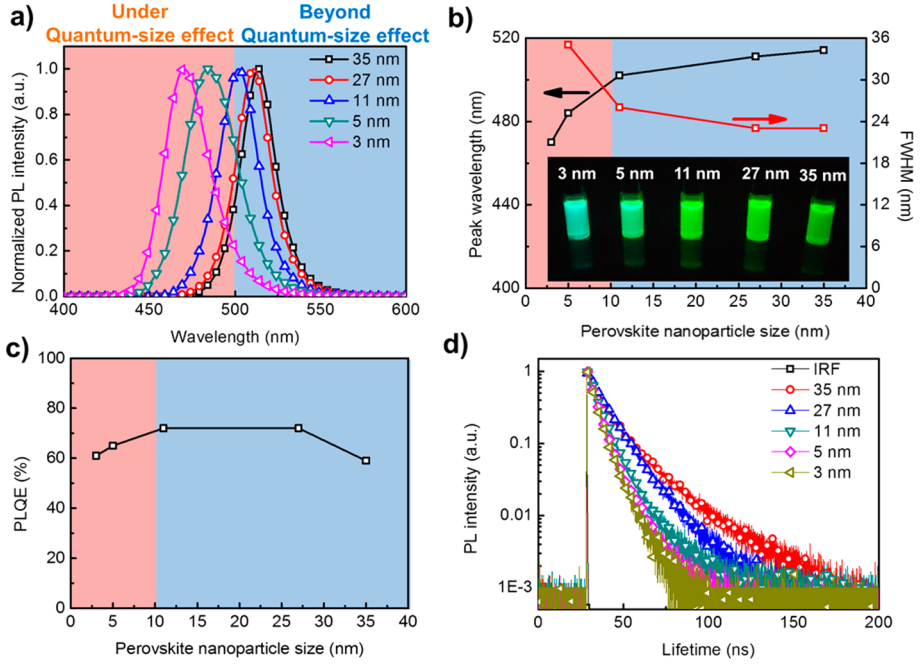

Figure 2. (a) PL spectra of perovskite NPs, (b) maximum PL peak wavelengths and fwhm of perovskite NPs and photograph of perovskite NPs under a λ = 350 nm Xe lamp (inset), (c) PLQE of the perovskite NPs under 400 nm excitation, and (d) PL lifetime curves of perovskite NPs obtained from TCSPC.

DOI: 10.1021/acsnano.6b07617
ACS Nano 2017, 11, 6586−6593

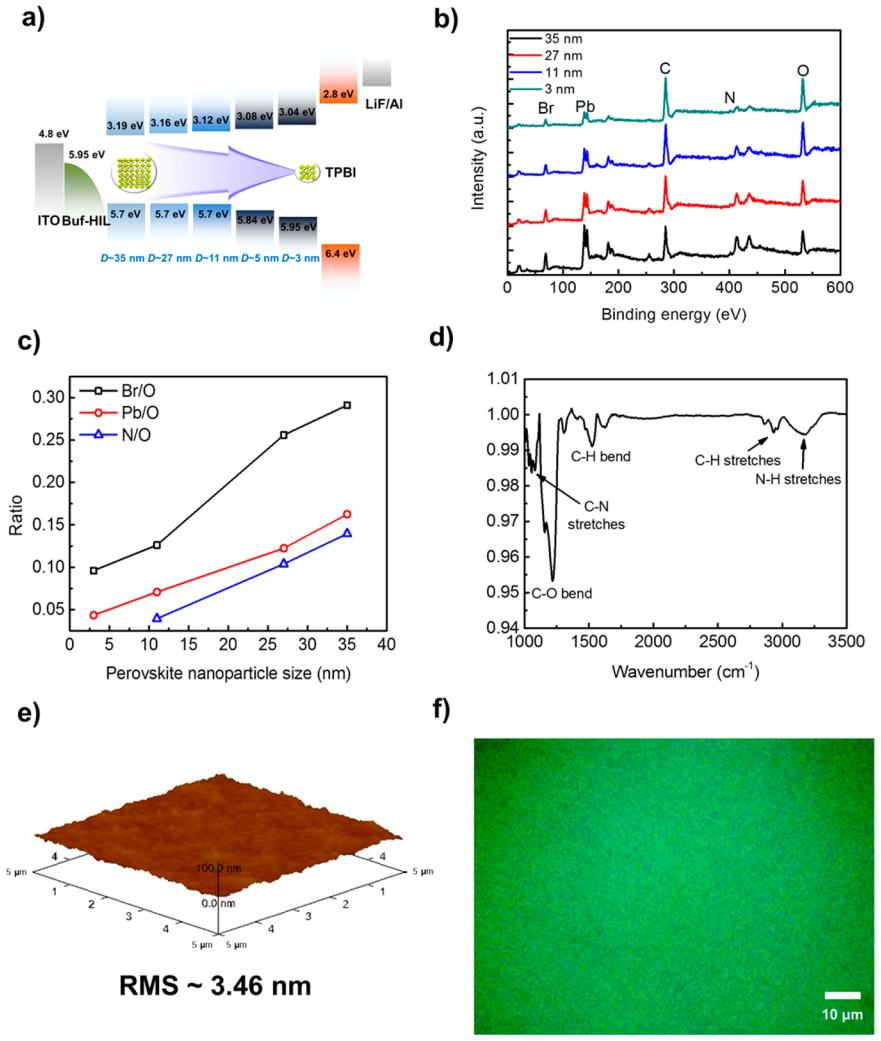

Figure 3. (a) Energy band diagram of perovskite NP-LEDs, (b) XPS survey spectra of perovskite NPs, (c) Br/O, Pb/O, and N/O ratios of perovskite NPs, (d) FT-IR spectrum of perovskite particle films, (e) AFM image of Buf-HIL/perovskite particle films, and (f) fluorescence microscope image of Buf-HIL/perovskite particle films under λ = 350 nm excitation.

structures depend on the unit crystal structure rather than on particle size. Perovskite NPs of size < D_B (*i.e.*, 5 and 3 nm QDs) showed a gradual blue shift in emission under UV illumination as the particle size decreased due to the quantum-size effect (inset of Figures 2b, S4). The PL peak positions of all perovskite NPs remained constant regardless of the excitation wavelength; this result indicates that they have a single lowest excited state (S_1), do not have any other PL centers (*e.g.*, from the ligand), and meet Kasha's rule (Figure S5).

Perovskite NCs with a size $\gtrsim D_B$ (*i.e.*, 11−27 nm) showed the highest PLQE (~72%) among perovskite NPs (Figure 2c). The high PLQE of perovskite NCs is due to the increased E_b and spatial exciton confinement in small NCs of size close to D_B, which increase the electron−hole wave function overlap and radiative recombination by reducing the thermal ionization and delocalization of excitons.[6−10] In contrast, perovskite QDs with a size less than D_B showed a gradually decreasing PLQE from ~65% for 5 nm QDs to ~62% for 3 nm QDs. We attribute this decrease to the increase in trap-assisted recombination of excitons at surface traps due to the larger surface-to-volume ratio because trap-assisted recombination is mainly related to the nonradiative recombination.[6,8,21,22,26] Due to the competing processes between thermal ionization ($\gg D_B$) and trapping of charge carriers at surface traps ($< D_B$), perovskite NCs with a size $\gtrsim D_B$ showed the highest PLQE and a sharp spectrum (small fwhm) with a constant PL position irrespective of particle size and size distribution, and thus can maximize the EL efficiency in LEDs.

To further understand the dynamics of excitons in perovskite NPs according to the size difference, we used time-correlated single-photon counting (TCSPC) to measure the PL lifetime of NPs (Figure 2d). All samples showed a much shorter average lifetime (τ_{av}) than did bulk perovskite films (~100 ns);[2] the reduction in lifetime indicates that PL decay of perovskite NPs mainly occurs by geminate electron−hole recombination due to increasing E_b and electron−hole overlap, rather than by free-carrier recombination.[6,7] As the size of the perovskite NPs decreased from 35 nm NPs to 3 nm NPs, the PL lifetime gradually decreased from 15.49 ns to 6.68 ns due to (i) enhanced spatial confinement of electron−hole pairs inside the perovskite NPs and (ii) increasing trap-assisted recombination of carriers at the surface traps.[2,21,22,26] In the perovskite NCs with a size $\geq D_B$ (~10 nm) (regime beyond the quantum size), spatial confinement of electron−hole pairs mainly occurred with decreasing NP size; thus, the PLQE of NPs gradually increased to a certain size close to the D_B (Figure 2c).

DOI: 10.1021/acsnano.6b07617
ACS Nano 2017, 11, 6586−6593

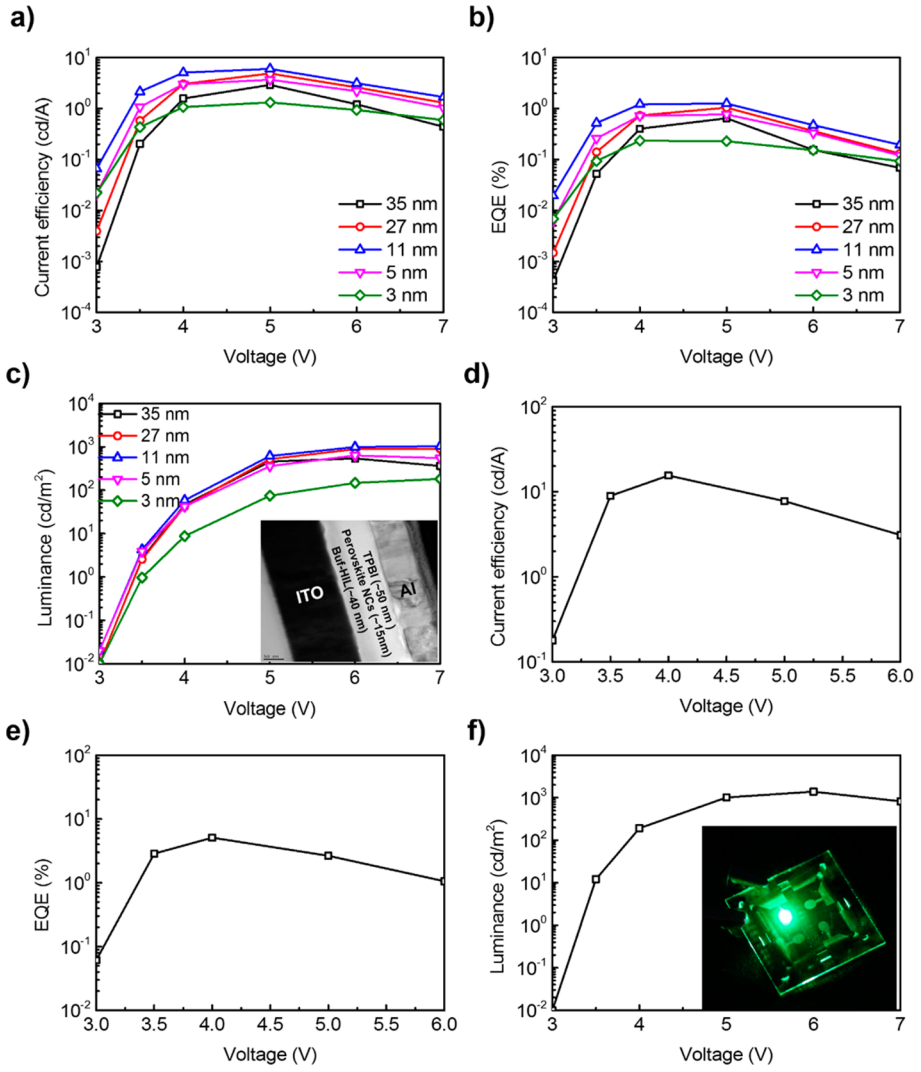

Figure 4. (a) CE characteristics, (b) EQE characteristics, and (c) luminance characteristics of perovskite NP-LEDs using various NPs and cross-sectional TEM image (inset); (d) CE characteristics, (e) EQE characteristics, and (f) luminance characteristics and photograph (inset) of perovskite NC-LEDs with a 30 nm thick perovskite particle layer.

However, in the perovskite QDs with a size < D_B (quantum size regime), trap-assisted recombination of carriers at the surface traps, which can mainly induce the nonradiative recombination of carriers, more severely occurred due to their large surface-to-volume ratio; thus, the PLQE of NPs tended to decrease with decreasing NP size (Figure 2c). Thus, our perovskite NPs with a size ≈ D_B showed the highest PLQE (~72%).

To measure the energy band structure of perovskite NPs, we conducted temperature (T)-dependent PL (Figures S6, S7), ultraviolet photoelectron spectroscopy (UPS) (Figure S8), and ultraviolet (UV)/visible absorption spectroscopy (Figure S9) of various NPs. As the perovskite NP size decreased, the E_b, IE, and optical band gap (*i.e.*, absorption onset) tended to increase from ~153 meV, ~5.7 eV, and ~2.35 eV for 35 nm NPs to ~319 meV, ~5.95 eV, and ~2.59 eV for 3 nm NPs, respectively. Thus, the band gap (*i.e.*, the gap between the valence band maximum and the conduction band minimum) also gradually increased from ~2.51 eV for 35 nm perovskite NPs to ~2.91 eV for 3 nm NPs (Figure 3a); these are similar to the inorganic QDs (<D_B).[30] These increasing band gaps of perovskite QDs (<10 nm) induced the quantum size effect and blue-shifted PL (Figure 2a,b and Figures S4, S5).

Furthermore, to relatively investigate the size reduction of perovskite NPs, we compared the peak intensity of C, O, Br, Pb, and N atoms in X-ray photoelectron spectroscopy (XPS) measurements. As the perovskite NP size decreased, the C and O peaks relatively increased, but the Br, Pb, and N peaks gradually decreased (Figure 3b,c and Figure S10).[6,31] We attribute these opposing changes to the increasing surface area, which contains a surface-capping agent (oleic acid), compared to the decreasing core perovskite nanostructure ($CH_3NH_3PbBr_3$). The surface characteristics were also identified using Fourier transform infrared (FT-IR) spectroscopy data (Figure 3d). We can clearly detect the C−N stretches (1020−1200 cm^{-1}) and C−O bend (1200−1300 cm^{-1}), which indicate the presence of hexylamine and oleic acid, respectively. The N−H stretches (3000−3300 cm^{-1}), C−H bend (1450−1550 cm^{-1}), and C−H stretches (2850−3000 cm^{-1}) also confirmed the presence of organic ligands (*e.g.*, hexylamine and oleic acid) and perovskite crystals ($CH_3NH_3PbBr_3$).

Perovskite particle films on Buf-HIL composed of PEDOT:PSS and perfluorinated polymeric acid (PFI), tetrafluoroethylene-perfluoro-3,6-dioxa-4-methyl-7-octenesulfonic acid copolymer, showed a uniform surface with a root-

DOI: 10.1021/acsnano.6b07617
ACS Nano 2017, 11, 6586−6593

mean-square roughness (r_{rms}) of 3.46 nm (Figure 3e). The uniform surface of Buf-HIL/perovskite particle films can reduce electrical shunt paths and leakage current in LED devices. However, perovskite particle films on conventional PEDOT:PSS HIL showed sparsely coated and aggregated particle structure and induced severe exciton quenching at the interface (Figure S11).[3] Furthermore, gradually increasing PFI concentration in Buf-HIL from the bottom surface to the top surface due to its self-organization can induce a gradually increasing work function of Buf-HIL from ~5.2 eV at the bottom surface to ~5.95 eV at the top surface, thus improving the hole injection capability to the perovskite particle emitting layer (EML) (Figure 3a).[3] A large proportion of PFI on top of Buf-HIL can also prevent exciton quenching at the PEDOT:PSS/perovskite particle film interface.[3] Therefore, Buf-HIL can increase the EL efficiencies of perovskite NP-LEDs not only by facilitating the hole injection and preventing exciton quenching at the PEDOT:PSS/perovskite particle film interface but also by inducing the uniform perovskite particle films possibly due to their low surface energy (~23 mN/m) (Figure S11 and Table S1).[3,32]

Uniform perovskite particle films on Buf-HIL maintained the sharp green PL peak of perovskite particle films at both RT and low T (Figure S12). Thus, perovskite particle films on Buf-HIL also maintained high PLQE (~60.5%) without any complex post-treatment; this value is only slightly lower than that of NPs in solution (PLQE ≈ 72%) and significantly higher than that of polycrystalline perovskite bulk film without an additional treatment (PLQE ≈ 2.4%, average size $\gtrsim \mu$m). The perovskite particle films on Buf-HIL also showed very uniform and bright PL under excitation at λ = 350 nm (Figure 3f).

LEDs based on perovskite NCs $\gtrsim D_B$ (11−27 nm) showed luminescence efficiencies (CE ≈ 4.88−6.02 cd/A and EQE ≈ 1.04−1.26%) that are higher than those of other devices (Figure 4a−c and Figure S13). The LEDs based on perovskite NPs $\gg D_B$ or $< D_B$ exhibited poorer luminescence efficiencies, which are consistent with the PLQE trend of emitting NPs, although some agglomeration of perovskite NPs occurs during the five-times spin-coating process of the NP solution (Figure S14). These low luminescence efficiencies of LEDs based on as-synthesized perovskite NPs $\gg D_B$ can be mainly ascribed to the large particle size in the deposited particle films (Figure S14), whereas the low efficiency in LEDs with as-synthesized NPs $< D_B$ is mainly due to the large amount of insulating ligand in the deposited particle films (Figure 3b,c and Figure S10). These luminescence efficiencies of LEDs based on various perovskite NPs are well reproduced in 10 randomly selected LED devices and also in LEDs without thermal annealing, although the overall luminescence efficiencies of LEDs without thermal annealing were much lower than those with thermal annealing, possibly due to the residual solvent and imperfect crystallinity in perovskite particle films (Figures S15, S16).[33]

To further confirm the size effects of as-synthesized perovskite NPs on the deposited perovskite particle films, we measured the τ_{av} of the deposited particle films. As the size of as-synthesized perovskite NPs increased, τ_{av} of the deposited perovskite particle films, as measured at the maximum PL peak (~520 nm), gradually increased from 43.75 ns for particle films fabricated by as-synthesized 3 nm NPs to 95.97 ns for particle films formed by as-synthesized 35 nm NPs (Figures S17, S18a). These results correspond well with the τ_{av} of as-synthesized perovskite NP solutions (Figure 2d) and thus confirm that the size of deposited perovskite particles in films was affected by the size of as-synthesized NPs. τ_{av} increased with increasing detection wavelength in perovskite particle films fabricated using as-synthesized NPs with large size (*i.e.*, 27 and 35 nm), but not in particle films fabricated using as-synthesized NPs with small size (*i.e.*, 3 and 5 nm) (Figure S18b−f). These increasing τ_{av} with increasing detection wavelength may be due to the large size distribution in perovskite particle films fabricated using large as-synthesized NPs.[34] These results also concur with the size distribution of the as-synthesized perovskite NPs (Figure 1d) and thus indicate that the relationship between size distribution and the particle size of deposited particle films corresponds to the same relationships in as-synthesized NPs. These results confirm that to maximize both the PLQE of perovskite NPs and luminescence efficiencies of NP-based LEDs, the size of as-synthesized NPs should be controlled to be ~D_B. Furthermore, these luminescence efficiencies of perovskite NC-LEDs are also much higher than those using conventional PEDOT:PSS (CE ≈ 0.117 cd/A) due to the homogeneous perovskite particle films with full coverage on Buf-HIL and improved hole injection capability and prevented exciton quenching at the PEDOT:PSS/perovskite particle film interface by using Buf-HIL (Table S1, Figures S11, S19). The average EML thickness of LEDs using 11 nm perovskite NCs is ~15 nm, and we assume that the average thickness of perovskite particle films in NP-LEDs in Figure 4a−c is around 1−1.5 monolayers (inset of Figure 4c).

We further optimized the luminescence efficiencies of perovskite NC-LEDs by increasing the thickness of the perovskite particle EML to ~30 nm. The perovskite NC-LEDs exhibited a very high maximum CE of 15.5 cd/A, an EQE of 5.09%, and a power efficiency (PE) of 12.17 lm/W without complex post-treatment and an additional layer (Figure 4d−f and Figure S20a,b). To our best knowledge, these efficiencies are the best in green LEDs based on colloidal organic−inorganic metal−halide perovskite NPs and comparable to the highest efficiencies in green LEDs based on colloidal all-inorganic metal−halide perovskite NPs (EQE ≈ 6.27%, CE ≈ 13.3 cd/A, PE ≈ 5.24 lm/W) including perovskite QDs and NCs to date.[35,36] The perovskite NC-LEDs exhibited very bright green emission (inset of Figure 4f). The sharp EL spectrum (fwhm ~22 nm) did not change with applied bias; this stability indicates that the Buf-HIL and electron-injecting TPBI layer efficiently facilitate charge injection into the perovskite particle layer and confine the injected holes and electrons in the EML (Figure S20c). The Commission Internationale de l'Éclairage coordinates were (0.088, 0.711), which are located outside the National Television System Committee's standard colors (inset of Figure S20c).[30]

CONCLUSIONS

In conclusion, we fabricated high-efficiency perovskite NC-LEDs with CE = 15.5 cd/A without any complex post-treatments and multilayers, which is the highest efficiency in green LEDs using organic−inorganic metal−halide perovskite NPs including perovskite QDs and NCs to date. To achieve a high EL efficiency in perovskite NPs, we (i) synthesized perovskite NC emitters with a dimension $\geq D_B$. Perovskite NCs can provide size-insensitive high color purity and high efficiency by preventing charge trapping at the surface defects or traps in NPs of size $< D_B$ and thermal ionization of excitons in NPs of size $\gg D_B$, respectively. Furthermore, we (ii) used Buf-HIL, which can efficiently prevent the exciton quenching at the PEDOT:PSS/perovskite particle film interface. Buf-HIL can

DOI: 10.1021/acsnano.6b07617
ACS Nano 2017, 11, 6586−6593

also give highly uniform perovskite particle films with complete film coverage, thus maximizing the PLQE (~60.5%) and EL efficiency of perovskite particle films.

This demonstration of high-efficiency perovskite NC-LEDs based on semiconducting perovskite NPs with a size $\geq D_B$ and Buf-HIL suggests a simple route to develop high-efficiency NP-LEDs that use inexpensive and size-insensitive emitters with high color purity and high efficiency, while inorganic QDs and perovskite QDs show size-sensitive emission colors and size-distribution-dependent color purity. Considering the low-cost processability, suitable dimensions for fine control for massive synthesis, size-insensitive light emission, applicability to many optoelectronics, and high PLQE of perovskite NCs, these methods described here can help to guide development of various light-emitting optoelectronic applications based on perovskite NCs.

METHODS AND EXPERIMENTAL DETAILS

Preparation of CH_3NH_3Br Precursor. CH_3NH_3Br was synthesized by reacting 50 mL of HBr (48% in water, Aldrich) with 30 mL of methylamine (40% in methanol, Junsei Chemical Co. Ltd.) in a 250 mL round-bottom flask. After evaporating the solvents, we collected the white precipitates. Then, we purified and recrystallized the products by using ethanol and diethyl ether.

Synthesis of Perovskite Nanoparticles. We dissolved 0.6 mmol of CH_3NH_3Br, 0.8 mmol of $PbBr_2$, and 80 μL of *n*-hexylamine in 20 mL of dimethylformamide (DMF) to form a clear transparent precursor solution. Then, 1 mL of precursor solution was dropped into 5 mL of a toluene solution containing predissolved oleic acid of different amounts, from 5 to 100 μL, with vigorous stirring. The solution changed to a yellow-green color immediately upon mixing. The solution was centrifuged at 3000 rpm for 10 min to remove large particles that settled down to the bottom of a Falcon tube. Then, we collected the perovskite NP solution by pouring the upper part of the solution into another vial except for the aggregated particles.

LED Fabrication. Indium tin oxide patterned glasses were sonicated twice in acetone and once in 2-isopropanol for 15 min each, then boiled in 2-isopropanol for 30 min and dried in an oven. After these steps, the glasses were treated with ozone for 10 min to make the surface hydrophilic. On the ozone-treated surface, Buf-HILs were spin-coated to make a layer of 40 nm thickness, then baked at 150 °C for 30 min. Each sample was transferred into a glovebox, and perovskite NP solutions that were dissolved in toluene were spin-coated with 3000 rpm for 90 s. The above spin-coating procedure was repeated five times. To fabricate thicker perovskite NP films, we spin-coated NP solutions with higher concentrations, which were synthesized by dripping a higher concentrated precursor solution (3.45 mmol of CH_3NH_3Br, 4.6 mmol of $PbBr_2$, and 460 μL of *n*-hexylamine in 20 mL of DMF) into oleic acid-dissolved toluene with vigorous stirring. After they were baked at 90 °C for 10 min, they were transferred to the vacuum chamber. Then, TPBI (50 nm), LiF (1 nm), and Al (100 nm) were thermally deposited sequentially in a high vacuum ($<10^7$ Torr) at rates of 1, 0.1, and 3 Å/s, respectively.

LED Characterization. The current–voltage luminance of the LEDs with a pixel area of 4 mm^2 was measured using a Keithley 2400 source meter and a Minolta CS2000 spectroradiometer.

Time-Correlated Single Photon Counting Measurement. A picosecond-pulse laser head (LDH-P-C-405B, PicoQuant) with a 405 nm excitation wavelength, ~150 fs pulse width, and 40 MHz repetition rate was used as an excitation source. The PL emission was spectrally resolved by using a monochromator (SP-2155, Acton). A TCSPC module (PicoHarp, PicoQuant) with an MCP-PMT (R3809U-50, Hamamatsu) was used for ultrafast detection.

Photoluminescence and Photoluminescence Quantum Efficiency Measurement. PL spectra and matrix were measured using a JASCO FP8500 spectrofluorometer. PLQEs of perovskite NP solutions were measured using the same spectrofluorometer equipped with a 100 mm integrating sphere (ILF-835) and calculated by Jasco SpectraManager II software. PLQEs of perovskite NC films were measured using a 407 nm blue diode laser with an excitation power of ~15 mW as an excitation source and Andor iDus DU490A InGaAs as a detector.

Transmission Electron Microscopy Measurement. Perovskite NP solutions in toluene were dropped on the carbon-coated copper mesh grids (CF200-Cu), which were purchased from Electron Microscopy Sciences. The transmission electron microscopy experiment was performed using a JEOL-JEM 2100F operating at an acceleration voltage of 200 kV.

ASSOCIATED CONTENT

Supporting Information

The Supporting Information is available free of charge on the ACS Publications website at DOI: 10.1021/acsnano.6b07617.

Additional TEM, XRD, PL matrix, temperature-dependent PL, UPS, UV/vis absorption, AFM, and LED performance (PDF)

AUTHOR INFORMATION

Corresponding Author

*E-mail: twlees@snu.ac.kr, taewlees@gmail.com.

ORCID

Christoph Wolf: 0000-0002-9340-9782
Aditya Sadhanala: 0000-0003-2832-4894
Sang Hyuk Im: 0000-0001-7081-5959
Tae-Woo Lee: 0000-0002-6449-6725

Notes

The authors declare no competing financial interest.

ACKNOWLEDGMENTS

Synthesis of nanoparticles, device fabrication and photophysical measurements were supported by Samsung Research Funding Center of Samsung Electronics under Project Number SRFC-MA-1402-07. Device optimization, electron microscopy and chemical analysis were also supported by the National Research Foundation of Korea (NRF) grant funded by the Korean government (Ministry of Science, ICT & Future Planning) (Grant No. NRF-2016R1A3B1908431). A.S. and R.H.F. gratefully acknowledge the support from EPSRC and the Indo-UK APEX project.

REFERENCES

(1) Tan, Z.-K.; Moghaddam, R. S.; Lai, M. L.; Docampo, P.; Higler, R.; Deschler, F.; Price, M.; Sadhanala, A.; Pazos, L. M.; Credgington, D.; Hanusch, F.; Bein, T.; Snaith, H. J.; Friend, R. H. Bright Light-Emitting Diodes Based on Organometal Halide Perovskite. *Nat. Nanotechnol.* **2014**, *9*, 687–692.

(2) Cho, H.; Jeong, S.-H.; Park, M.-H.; Kim, Y.-H.; Wolf, C.; Lee, C.-L.; Heo, J. H.; Sadhanala, A.; Myoung, N.; Yoo, S.; Im, S. H.; Friend, R. H.; Lee, T.-W. Overcoming the Electroluminescence Efficiency Limitations of Perovskite Light–Emitting Diodes. *Science* **2015**, *350*, 1222–1225.

(3) Kim, Y.-H.; Cho, H.; Heo, J. H.; Kim, T.-S.; Myoung, N.; Lee, C.-L.; Im, S. H.; Lee, T.-W. Multi-Colored Organic/Inorganic Hybrid Perovskite Light–Emitting Diodes. *Adv. Mater.* **2015**, *27*, 1248–1254.

(4) Xiao, Z.; Kerner, R. A.; Zhao, L.; Tran, N. L.; Lee, K. M.; Koh, T.-W.; Scholes, G. D.; Rand, B. P. Efficient Perovskite Light-Emitting Diodes Featuring Nanometre-Sized Crystallites. *Nat. Photonics* **2017**, *11*, 108–115.

(5) Heo, J. H.; Song, D. H.; Im, S. H. Planar $CH_3NH_3PbBr_3$ Hybrid Solar Cells with 10.4% Power Conversion Efficiency, Fabricated by Controlled Crystallization in the Spin-Coating Process. *Adv. Mater.* **2014**, *26*, 8179–8183.

DOI: 10.1021/acsnano.6b07617
ACS Nano 2017, 11, 6586–6593

(6) Zhang, F.; Zhong, H.; Chen, C.; Wu, X.-G.; Hu, X.; Huang, H.; Han, J.; Zou, B.; Dong, Y. Brightly Luminescent and Color-Tunable Colloidal $CH_3NH_3PbX_3$ (X= Br, I, Cl) Quantum Dots: Potential Alternatives for Display Technology. *ACS Nano* **2015**, *9*, 4533−4542.
(7) Kim, Y.-H.; Cho, H.; Lee, T.-W. Metal Halide Perovskite Light Emitters. *Proc. Natl. Acad. Sci. U. S. A.* **2016**, *113*, 11694−11702.
(8) Huang, H.; Susha, A. S.; Kershaw, S. V.; Hung, T. F.; Rogach, A. L. Control of Emission Color of High Quantum Yield $CH_3NH_3PbBr_3$ Perovskite Quantum Dots by Precipitation Temperature. *Adv. Sci.* **2015**, *2*, 1500194.
(9) Zheng, K.; Zhu, Q.; Abdellah, M.; Messing, M. E.; Zhang, W.; Generalov, A.; Niu, Y.; Ribaud, L.; Canton, S. E.; Pullerits, T. Exciton Binding Energy and the Nature of Emissive States in Organometal Halide Perovskites. *J. Phys. Chem. Lett.* **2015**, *6*, 2969−2975.
(10) Schmidt, L. C.; Pertegás, A.; González-Carrero, S.; Malinkiewicz, O.; Agouram, S.; Espallargas, G. M.; Bolink, H. J.; Galian, R. E.; Pérez-Prieto, J. Nontemplate Synthesis of $CH_3NH_3PbBr_3$ Perovskite Nanoparticles. *J. Am. Chem. Soc.* **2014**, *136*, 850−853.
(11) Kim, Y.; Yassitepe, E.; Voznyy, O.; Comin, R.; Walters, G.; Gong, X.; Kanjanaboos, P.; Nogueira, A. F.; Sargent, E. H. Efficient Luminescence from Perovskite Quantum Dot Solids. *ACS Appl. Mater. Interfaces* **2015**, *7*, 25007−25013.
(12) Jang, D. M.; Park, K.; Kim, D. H.; Park, J.; Shojaei, F.; Kang, H. S.; Ahn, J.-P.; Lee, J. W.; Song, J. K. Reversible Halide Exchange Reaction of Organometal Trihalide Perovskite Colloidal Nanocrystals for Full-Range Band Gap Tuning. *Nano Lett.* **2015**, *15*, 5191−5199.
(13) Anikeeva, P. O.; Halpert, J. E.; Bawendi, M. G.; Bulović, V. Quantum Dot Light-Emitting Devices with Electroluminescence Tunable over the Entire Visible Spectrum. *Nano Lett.* **2009**, *9*, 2532−2536.
(14) Ling, Y.; Yuan, Z.; Tian, Y.; Wang, X.; Wang, J. C.; Xin, Y.; Hanson, K.; Ma, B.; Gao, H. Bright Light-Emitting Diodes Based on Organometal Halide Perovskite Nanoplatelets. *Adv. Mater.* **2016**, *28*, 305−311.
(15) Li, G.; Rivarola, F. W. R.; Davis, N. J. L. K.; Bai, S.; Jellicoe, T. C.; Peña, F. D. L.; Hou, S.; Ducati, C.; Gao, F.; Friend, R. H.; Greenham, N. C.; Tan, Z.-K. Highly Efficient Perovskite Nanocrystal Light-Emitting Diodes Enabled by a Universal Crosslinking Method. *Adv. Mater.* **2016**, *28*, 3528−3534.
(16) Deng, W.; Xu, X.; Zhang, X.; Zhang, Y.; Jin, X.; Wang, L.; Lee, S.-T.; Jie, J. Organometal Halide Perovskite Quantum Dot Light-Emitting Diodes. *Adv. Funct. Mater.* **2016**, *26*, 4797−4802.
(17) Liang, D.; Peng, Y.; Fu, Y.; Shearer, M. J.; Zhang, J.; Zhai, J.; Zhang, Y.; Hamers, R. J.; Andrew, T. L.; Jin, S. Color-Pure Violet-Light-Emitting Diodes Based on Layered Lead Halide Perovskite Nanoplates. *ACS Nano* **2016**, *10*, 6897−6904.
(18) Kumar, S.; Jagielski, J.; Yakunin, S.; Rice, P.; Chiu, Y.-C.; Wang, M.; Nedelcu, G.; Kim, Y.; Lin, S.; Santos, E. J. G.; Kovalenko, M. V.; Shih, C.-J. Efficient Blue Electroluminescence Using Quantum-Confined Two-Dimensional Perovskites. *ACS Nano* **2016**, *10*, 9720−9729.
(19) Xing, J.; Yan, F.; Zhao, Y.; Chen, S.; Yu, H.; Zhang, Q.; Zeng, R.; Demir, H. V.; Sun, X.; Huan, A.; Xiong, Q. High-Efficiency Light-Emitting Diodes of Organometal Halide Perovskite Amorphous Nanoparticles. *ACS Nano* **2016**, *10*, 6623−6630.
(20) Zhang, X.; Lin, H.; Huang, H.; Reckmeier, C.; Zhang, Y.; Choy, W. C. H.; Rogach, A. L. Enhancing the Brightness of Cesium Lead Halide Perovskite Nanocrystal Based Green Light-Emitting Devices through the Interface Engineering with Perfluorinated Ionomer. *Nano Lett.* **2016**, *16*, 1415−1420.
(21) Ma, G.; Tang, S.-H.; Sun, W.; Shen, Z.; Huang, W.; Shi, J. Size-Dependent Excited State Properties of CdS Nanocrystals. *Phys. Lett. A* **2002**, *299*, 581−585.
(22) De Quilettes, D. W.; Vorpahl, S. M.; Stranks, S. D.; Nagaoka, H.; Eperon, G. E.; Ziffer, M. E.; Snaith, H. J.; Ginger, D. S. Impact of Microstructure on Local Carrier Lifetime in Perovskite Solar Cells. *Science* **2015**, *348*, 683−686.
(23) Kwon, W.; Lee, G.; Do, S.; Joo, T.; Rhee, S.-W. Size-Controlled Soft-Template Synthesis of Carbon Nanodots toward Versatile Photoactive Materials. *Small* **2014**, *10*, 506−513.
(24) Im, J.-H.; Jang, I.-H.; Pellet, N.; Grätzel, M.; Park, N.-G. Growth of $CH_3NH_3PbI_3$ Cuboids with Controlled Size for High-Efficiency Perovskite Solar Cells. *Nat. Nanotechnol.* **2014**, *9*, 927−932.
(25) Jeon, T.; Jin, H. M.; Lee, S. H.; Lee, J. M.; Park, H. I.; Kim, M. K.; Lee, K. J.; Shin, B.; Kim, S. O. Laser Crystallization of Organic−Inorganic Hybrid Perovskite Solar Cells. *ACS Nano* **2016**, *10*, 7907−7914.
(26) Tachikawa, T.; Karimata, I.; Kobori, Y. Surface Charge Trapping in Organolead Halide Perovskites Explored by Single-Particle Photoluminescence Imaging. *J. Phys. Chem. Lett.* **2015**, *6*, 3195−3201.
(27) Di, D.; Musselman, K. P.; Li, G.; Sadhanala, A.; Ievskaya, Y.; Song, Q.; Tan, Z.-K.; Lai, M. L.; MacManus-Driscoll, J. L.; Greenham, N. C.; Friend, R. H. Size-Dependent Photon Emission from Organometal Halide Perovskite Nanocrystals Embedded in an Organic Matrix. *J. Phys. Chem. Lett.* **2015**, *6*, 446−450.
(28) Galkowski, K.; Mitioglu, A.; Miyata, A.; Plochocka, P.; Portugall, O.; Eperon, G. E.; Wang, J. T.-W.; Stergiopoulos, T.; Stranks, S. D.; Snaith, H. J.; Nicholas, R. J. Determination of the Exciton Binding Energy and Effective Masses for Methylammonium and Formamidinium Lead Tri-Halide Perovskite Semiconductors. *Energy Environ. Sci.* **2016**, *9*, 962−970.
(29) Brus, L. Electronic Wave Functions in Semiconductor Clusters: Experiment and Theory. *J. Phys. Chem.* **1986**, *90*, 2555−2560.
(30) Kwak, J.; Bae, W. K.; Lee, D.; Park, I.; Lim, J.; Park, M.; Cho, H.; Woo, H.; Yoon, D. Y.; Char, K.; Lee, S.; Lee, C. Bright and Efficient Full-Color Colloidal Quantum Dot Light-Emitting Diodes using an Inverted Device Structure. *Nano Lett.* **2012**, *12*, 2362−2366.
(31) Gonzalez-Carrero, S.; Galian, R. E.; Pérez-Prieto, J. Maximizing the Emissive Properties of $CH_3NH_3PbBr_3$ Perovskite Nanoparticles. *J. Mater. Chem. A* **2015**, *3*, 9187−9193.
(32) Han, T.-H.; Choi, M.-R.; Woo, S.-H.; Min, S.-Y.; Lee, C.-L.; Lee, T.-W. Molecularly Controlled Interfacial Layer Strategy Toward Highly Efficient Simple-Structured Organic Light-Emitting Diodes. *Adv. Mater.* **2012**, *24*, 1487−1493.
(33) Kim, Y.-H.; Cho, H.; Heo, J. H.; Im, S. H.; Lee, T.-W. Effects of Thermal Treatment on Organic-Inorganic Hybrid Perovskite Films and Luminous Efficiency of Light-Emitting Diodes. *Curr. Appl. Phys.* **2016**, *16*, 1069−1074.
(34) Swarnkar, A.; Chulliyil, R.; Ravi, V. K.; Irfanullah, M.; Chowdhury, A.; Nag, A. Colloidal $CsPbBr_3$ Perovskite Nanocrystals: Luminescence beyond Traditional Quantum Dots. *Angew. Chem.* **2015**, *127*, 15644−15648.
(35) Li, J.; Xu, L.; Wang, T.; Song, J.; Chen, J.; Xue, J.; Dong, Y.; Cai, B.; Shan, Q.; Han, B.; Zeng, H. 50-Fold EQE Improvement up to 6.27% of Solution-Processed All-Inorganic Perovskite $CsPbBr_3$ QLEDs *via* Surface Ligand Density Control. *Adv. Mater.* **2017**, *29*, 1603885.
(36) Kim, Y.-H.; Lee, G.-H.; Kim, Y.-T.; Wolf, C.; Yun, H. J.; Kwon, W.; Park, C. G.; Lee, T.-W. High Efficiency Perovskite Light-Emitting Diodes of Ligand-Engineered Colloidal Formamidinium Lead Bromide Nanoparticles. *Nano Energy* **2017**, *38*, 51−58.

DOI: 10.1021/acsnano.6b07617
ACS Nano 2017, 11, 6586−6593